https://doi.org/10.1016/j.compscitech.2021.108645

Modeling the Stress and Resistance Relaxation of Conductive Composites-coated Fabric Strain Sensors

Xi WANG[1, #], Bao YANG[2, #], Qiao LI[3,], Fei WANG[2], Xiao-ming TAO[2,*]*

[1] Engineering Research Center of Digitized Textile & Apparel Technology, Ministry of Education, College of Information Science and Technology, Donghua University, Shanghai 201620, China

[2] Research Centre of Smart Wearable and Intelligent Textile and Apparel, Institute of Textiles and Clothing, The Hong Kong Polytechnic University, Kowloon, Hong Kong, China

[3] Key Laboratory of Textile Science & Technology of Ministry of Education, College of Textiles, Donghua University, Shanghai 201620, China

*Correspondence: qiaoli@dhu.edu.cn; xiao-ming.tao@polyu.edu.hk

# These first authors contributed equally.

Abstract

Electrical relaxation of flexible sensors using the conductive polymer composites as sensing materials has been constantly reported as major obstacle for accurate measurement, yet still roughly characterized by mechanical relaxation rather than an effective underlying mechanism. In this work, fabric strain sensors based on carbon-particle-filled conductive polymer and knitted fabric substrate were studied. A serial mechanical model of the sensor was established according to its structure, and then extended to an electromechanical model by introducing strain-resistance properties for mechanical elements. Methods were elaborated on extracting the mechanical, electrical and status parameters of the model. Tests were conducted on 5 randomly-chosen samples. The model was firstly determined for each sample using proposed methods and then implemented to predict resistance response during relaxations. Results show that the relative mean error of the predicted resistance was only 0.2%, with an averaged

determination of fit 0.9230. The correlation between predicted and measured resistance was observed 0.9783 on average. Conclusion can be drawn that the model is effective to characterize the sensing mechanism and resistance relaxation of the fabric strain sensors.

Keywords: A:Fabrics/textiles; A:Polymer-matrix composites; B: Electro-mechanical behavior; C: Material modeling; C:Stress relaxation.

1. Introduction

Conductive polymer composites are ideal sensing materials, especially for wearable sensing applications. Thanks to the merits of low modulus, lightweight, excellent flexibility, easy processing, and favorable sensitivity of electrical resistance to mechanical deformation, they have been frequently utilized to develop numerous flexible sensing elements. For instance, the high-performance smart flexible strain sensors based on conductive polymer composites have been frequently reported in human movement detection, health monitoring, soft robotic skin, and human-machine interaction [1-5]. Moreover, the conductive polymer composites have also been further incorporated in the novel fabric sensing technologies. In recent years, 2 categories of fabric strain sensors that have been frequently reported [6-10], i.e., conductive elastomer (CE) and knitted piezoresistive fabric (KPF), realized by screen-printing CE on fabrics and knitting conductive yarns into fabrics, respectively. Those fabric sensors can easily conform to curved human skin and be seamlessly embedded in apparels, forming a number of functional and intelligent wearable apparatus.

However, those sensors are difficult to achieve a stable response at a given extension/road due to the rheological property of conductive polymer composites. Stress relaxation of viscoelastic materials, i.e., stress decreases with time in response to the constant applied strain, has been frequently observed and discussed [11-13]. This nonlinear behavior of stress and strain for a viscoelastic material is commonly known and reported by either stress relaxation or creep. Since CE and KPF sensors consist of fabric/fiber substrate instead of just pure conductive polymer composites, constraints between fabric/fiber and conductive polymer would definitely affect the mechanical behavior of stress. Characteristics of stress relaxation of those sensors shall be

determined or verified, which has not been elaborately addressed according to the review of up-to-date relative works.

Moreover, the objective fact that resistance of sensors also ‘relaxes’ simultaneously with stress at fixed strain, described by the term ‘resistance relaxation’ [14, 15], has been restricting those sensors in qualitative instead of quantitative and accurate temporal sensing applications. Prior to compensating sensors’ measurements or model optimization for the sensing behavior of the sensors, some researches on characterizing the resistance relaxation of conductive polymers have been conducted. Generally, the temporal stress relaxation of carbon black loaded vulcanizates or carbon black filled elastomers can be fitted using an exponential function with minus indexes and simulated with spring-dashpot systems [16-18]. As per the electrical resistance, however, there is a mere phenomenological conclusion that the electrical resistance and stress of the composite seemed decreasing in similar patterns during fixed strains. To name some of those researches, Wang’s group [19-23] studied carbon black filled silicone rubber, considered the sensing material as Maxwell and Voigt models and incorporated a linear combination of two negative exponential functions to fit both the data of the compressive stress relaxation and resistance relaxation, since it’s claimed that the mathematical models of the decompressive stress relaxation and the decompressive resistance relaxation are similar in trend. The effects of the instantaneous pressure decrement on the relaxation indices and coefficients of the fitted function were studied, with results explained only qualitatively by analyzing the changes in polymer chain segments and effective conductive paths of the composite. Zheng’s group [24-29] utilized a combination of exponential and linear functions to characterize temporal changes in the resistance and stress of conductive polymer over a limited time range at fixed strains, where the parameters in the model depend on the level of compression. However and to date, almost all relative works tended to believe that relaxations of stress and resistance are under the same or similar unknown physics bases, very few researches looked deep into the real mechanism of resistance relaxation of conductive polymer composites or fabric sensors based on conductive polymers.

Hence in this paper, CE fabric strain sensors based on carbon-particle-filled polymer were studied through mechanical and electrical modeling. A mechanical model of CE fabric strain sensors will be proposed firstly. Sectional gauge factors and status parameters will be included to provide an electromechanical mechanism of the FSSs. The model will be determined for each FSS through parameter identification and applied for prediction of variance in resistance for FSS during relaxation. The verification of the model will then be conducted by analyzing the error of the predicted resistance during relaxation. This work generally presents a physical mechanism of relaxation in electrical resistance of FSS, as well as establishes a reasonable and reliable connection between stress relaxation and resistance relaxation.

2. Mathematical models for stress and resistance relaxation

2.1 Fabric strain sensors

In this paper, fabric strain sensors (FSSs, provided by AdvanPro Limited, Hong Kong, China) were studied. The image and schematic structure of the FSSs are shown in **Figure 1**. The FSS consists of a conductive film, elastic knitted fabric, woven fabric, and silver wires. The conductive film was manufactured by dispersing carbon nanoparticles (CNP) in elastomer composites of silicone rubber (SE) and silicone oil (SO). The use of SO can effectively decrease the modulus of the composites to less than 1 MPa, without affecting the elongation capability. However, the viscosity of the conductive polymer composite can cause the resistance-strain hysteresis to as high as 17%. Therefore, knitted fabrics made from highly elastic fibers were introduced in the structure as a base for the sensitive conductive composite film. The sensors have shown low modulus, marginal strain-rate dependent, small humidity effect, and good linearity and repeatability in strain up to 50%.

The response delay of such FSSs has been studied by Wang [30] and revealed as 0.1 ~ 0.3 ms, negligible for capturing human movements. Calibration of the FSSs was conducted with INSTRON 5944 (Instron Corp., USA) within the working range of 5% ~ 60% strain [8] along the tensile direction/length direction. In multiple times of previous applications, the FSSs were observed with a strain measurement error of only 5% and controlled hysteresis of less than 3% in cyclic tests within the working range and loading speed of 60 mm/min. Such FSSs have been incorporated in various applications of

wearable electronics and smart textiles as sensing elements [8, 30, 31] due to the merits, including large deformation ability with a large measurement range from zero to over 60%, flexible, soft and good fatigue resistance. However, for low-speed loading or holding at certain strains, resistance relaxation starts to contribute more errors into strain measurement.

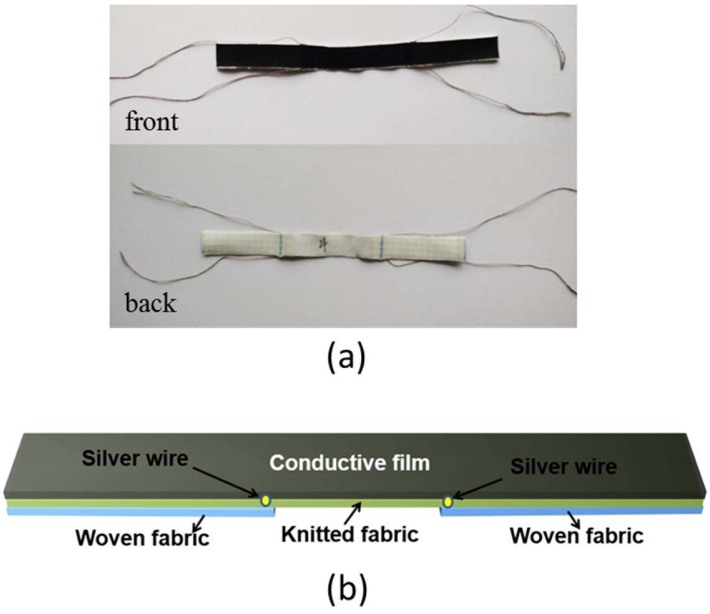

Figure 1 Real picture (a) and schematic structure (b) of fabric strain sensors

2.2 Mechanical model of the sensors

Relaxations of pure conductive composites materials have been frequently reported. While under tension with fixed distance, the stress distribution of each slice tends to relax to adapt a lower energy level while the strain distribution simultaneously accommodate the stress, in the process of which the electrical resistance varies due to changed distances between conductive particles within conductive film. Hence, stress relaxations of pure conductive material have been reported as can be well-characterized by parallel mechanical models with spring-Maxwell elements [32-34] (**Figure 2a**), where the tension relaxation of the FSSs can be characterized using the following equation

$$\sigma(t) = \sigma(\infty) + \sum_i \sigma_i \cdot e^{-\lambda_i t} \tag{1}$$

where $\sigma(\infty)$ denotes the limitation of stress at infinite time, σ_i is coefficients, λ_i is the exponential coefficient or relaxation index. The coefficients can be obtained through parameter identification with real temporal stress.

Although parallel mechanical models are very convenient to use, it's quite difficult to be connected to electrical responses with reasonable physical significance. Moreover, for the printed/coated sensors with fabric base (Figure 1), the style of tensile deformation has been largely affected by the structure of the knitted fabric substrate. As can be seen in **Figure 2b**, the surface of the sensor (conductive film) reveals obvious grid pattern, resembling that of the knitted fabric underneath. Thanks to the fabric substrate, width of grids changed slightly while the length increased significantly under longitudinal tension. In this condition, stress and electrical relaxation of the sensor (composites and fabric substrates together) can be regarded as caused by the strain redistribution in the length direction. Hence, the sensor can be seen as comprised by multiple identical parallel slices in the length direction, where each slice is a fundamental rheological element containing constant number of conductive tunnels. For one single longitudinal element, the regions adhered to fibers are with higher modulus and perform more like a spring-dashpot (rheological) while the regions between fibers are with lower modulus, respond fast to applied strain and act more like spring (elastic).

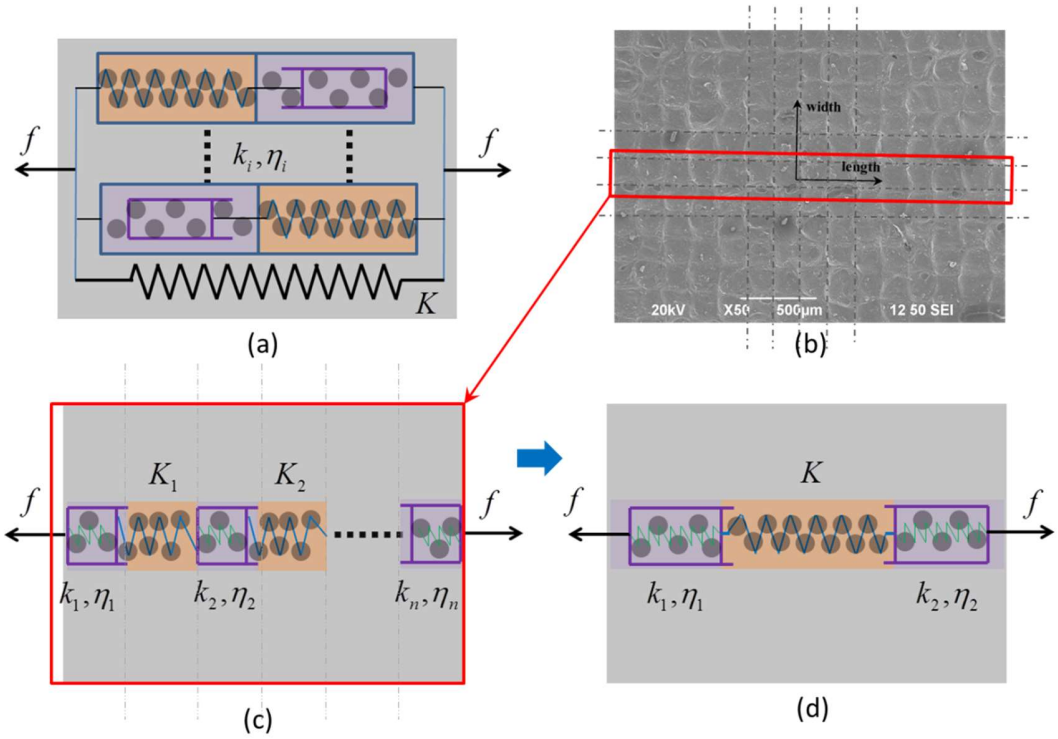

Figure 2 Mechanical models of FSSs: (a) Commonly-used parallel mechanical model, (b)Surface of the printed fabric strain sensor; (c) Serial mechanical model of FSS and (d) The 2-order serial model

Hence, it's reasonable to incorporate a serial model of the sensor constructed by spring and Voight elements, as shown in **Figure 2c**. In this model, the springs represent subsections with a lower modulus that can response to strains instantly (i.e., regions adhered to fibers), while the Voight element represents that with higher modulus and slower response to strains (i.e., regions between fibers). It's worth mentioning that this serial model is naturally a complex simulation model, but can be further simplified to only a limited number of differentiated elements. To understand this, assume the FSSs are fabricated with perfectly periodical knitted fabric substrate and perfectly evenly coated conductive composites. In this condition, all elements of the same type are identical and can be combined, leading to a 2-unit model with only one combined Voight element and one combined spring element. This is a 1-order model since there is only one relaxation term according to **equation (1)**. It's not this case, however, for real sensors. Due to many reasons, elements are not ideally identical, and more feature groups shall be considered to reflect the differences among Voight elements, leading to differentiated

combined elements (naturally significantly different from each other) in a higher-order model, where the order depends on the conformity of the model to actual data. It's not direct but easy to understand that howsoever high order the model is, the temporal stress can always be expressed in the same form as in above **equation (1)**, i.e., by the summation of a number of relaxation terms, only that σ_i and λ_i are of totally different physical significances. Excellences of the model are that, not only it can successfully reflect the deformation styles of the sensors, but also that in this serial configuration, tension relaxation of the sensor can be represented by strain shift of elements, which can be then related to variation of electrical responses, so that the mechanical-electrical mechanism can be theoretically derived. In one word, this serial model can provide an approximation of the rheological behavior of the polymer-coated fabric sensors.

Since specifically for FSSs, it has been empirically found in previous work and repeatedly confirmed that 2 relaxation terms were good enough to characterize the short-term temporal stress relaxation in short-time (with r^2 higher than 0.995) [35], the proposed serial model can be largely simplified to be with only 3 subsections (1 spring element and 2 Voigt elements, as in **Figure 2d**). Given the stiffness and damping coefficient for the subsections, the tension of this model can be easily derived after solving the displacements of two pistons of dashpots, which are governed by

$$\begin{cases} K \cdot \left[l_0 - \left(s_1 + s_2 \right) \right] = k_1 \cdot s_1 + \eta_1 \cdot \dot{s}_1 \\ k_1 \cdot s_1 + \eta_1 \cdot \dot{s}_1 = k_2 \cdot s_2 + \eta_2 \cdot \dot{s}_2 \\ s_1 \big|_{t=0} = s_{1,0}, s_2 \big|_{t=0} = \mathrm{s}_{2,0} \end{cases} \tag{2}$$

where K is the stiffness of spring element in the middle, k_i, η_i are stiffness and damping coefficients for the Voight elements at both ends, l_0 is the initial elongation of the spring before relaxation happens, s_1, s_2 are displacements of the 2 pistons of dashpots, also the displacements of the interface between adjacent subsections. Boundary condition of s_1, s_2 at time 0 are assumed $s_{1,0}, \mathrm{s}_{2,0}$, respectively. With the above differential equations, the time-dependent displacement s_1, s_2 can be solved and expressed by

$$\begin{cases} s_1 = C_{11}e^{-\lambda_1 t} + C_{12}e^{-\lambda_2 t} + C_{13} \\ s_2 = C_{21}e^{-\lambda_1 t} + C_{22}e^{-\lambda_2 t} + C_{23} \end{cases} \tag{3}$$

The parameters can be obtained using

$$\lambda_1 = \frac{1}{2}\left(\varphi_{11} + \varphi_{12} + \varphi_{21} + \varphi_{22} - \psi\right);$$

$$\lambda_2 = \frac{1}{2}\left(\varphi_{11} + \varphi_{12} + \varphi_{21} + \varphi_{22} + \psi\right);$$

$$C_{11} = \frac{C_{13} - s_{10} - \dfrac{k_2 - \eta_2\lambda_2}{k_1 - \eta_1\lambda_2}\left(C_{23} - s_{20}\right)}{\dfrac{k_2 - \eta_2\lambda_2}{k_1 - \eta_1\lambda_2} \cdot \dfrac{k_1 - \eta_1\lambda_1}{k_2 - \eta_2\lambda_1} - 1}; C_{21} = \frac{C_{23} - s_{20} - \dfrac{k_1 - \eta_1\lambda_2}{k_2 - \eta_2\lambda_2}\left(C_{13} - s_{10}\right)}{\dfrac{k_1 - \eta_1\lambda_2}{k_2 - \eta_2\lambda_2} \cdot \dfrac{k_2 - \eta_2\lambda_1}{k_1 - \eta_1\lambda_1} - 1};$$

$$C_{12} = \frac{C_{13} - s_{10} - \dfrac{k_2 - \eta_2\lambda_1}{k_1 - \eta_1\lambda_1}\left(C_{23} - s_{20}\right)}{\dfrac{k_1 - \eta_1\lambda_2}{k_2 - \eta_2\lambda_2} \cdot \dfrac{k_2 - \eta_2\lambda_1}{k_1 - \eta_1\lambda_1} - 1}; C_{22} = \frac{C_{23} - s_{20} - \dfrac{k_1 - \eta_1\lambda_1}{k_2 - \eta_2\lambda_1}\left(C_{13} - s_{10}\right)}{\dfrac{k_2 - \eta_2\lambda_2}{k_1 - \eta_1\lambda_2} \cdot \dfrac{k_1 - \eta_1\lambda_1}{k_2 - \eta_2\lambda_1} - 1};$$

$$C_{13} = \frac{l_0}{1 + \dfrac{k_1}{k_2} + \dfrac{k_1}{K}}; C_{23} = \frac{l_0}{1 + \dfrac{k_2}{k_1} + \dfrac{k_2}{K}}.$$

where

$$\varphi_{11} = \frac{k_1}{\eta_1}; \varphi_{12} = \frac{K}{\eta_1}; \varphi_{21} = \frac{k_2}{\eta_2}; \varphi_{22} = \frac{K}{\eta_2};$$

$$\psi = \sqrt{\left(\varphi_{11} + \varphi_{12} - \varphi_{21} - \varphi_{22}\right)^2 + 4\varphi_{12}\varphi_{22}}.$$

Hence, once s_1, s_2 are determined, the tension of the sensor during relaxation can be derived as

$$\begin{aligned} F &= k_1 \cdot s_1 + \eta_1 \cdot \dot{s}_1 \\ &= \left(k_1 - \eta_1\lambda_1\right)C_{11}e^{-\lambda_1 t} + \left(k_1 - \eta_1\lambda_2\right)C_{12}e^{-\lambda_2 t} + k_1 \cdot C_{13} \\ &= \sigma\left(\infty\right) + \sigma_1 \cdot e^{-\lambda_1 t} + \sigma_2 \cdot e^{-\lambda_2 t} \end{aligned} \tag{4}$$

where $\sigma\left(\infty\right) = \dfrac{l_0}{\dfrac{1}{k_1} + \dfrac{1}{k_2} + \dfrac{1}{K}}$, $\sigma_1 = \left(k_1 - \eta_1\lambda_1\right)C_{11}$, $\sigma_2 = \left(k_1 - \eta_1\lambda_2\right)C_{12}$.

2.3 Electromechanical model of the sensors

This proposed serial mechanical model as above can be further extended to yield an electromechanically model of the FSSs, which involves tension, electrical resistance, and the connection between. The basic idea is to consider the time-dependent displacement of the pistons of the dashpots, which are attributed to the increase of resistance for the 1st and 3rd sections of the spring-dashpot element as well as decrease of resistance for the middle section of spring elements. According to the theory of tunneling current [36],

$$R = \left(\frac{N_p}{N_t} \right) \frac{8\pi hs}{3a^2 \gamma e^2} \exp(\gamma s) \tag{5}$$

where R is the equivalent resistance of the composite/FSS; N_p is the number of conductive particles forming a single conductive path parallel to the conductive direction; N_t is the number of conductive pathways; h is the Plank's constant; s is the least distance between conductive particles or domains; a^2 is the effective cross-sectional area in which the tunneling current passes through; e is the electron charge, and the constant γ is defined as $\gamma = \frac{4\pi}{h}\sqrt{2m\varphi}$, in which m is the electron mass and φ is the height of potential barrier between adjacent conductive particles. This equation generally governs the correlation between elongation and resistance for CE based on polymers filled with conductive particles inside. Please note that the above equation of tunneling resistance is applicable for elongated CE in FSS under the condition that the number of conductive particles in a conductive track as well as that the numbers of conductive tracks remain the same. Consider a strain exerted on FSS, the resistance can be given as

$$R = \left(\frac{N_p}{N_t} \right) \frac{8\pi hs(1+\varepsilon)}{3a^2 \gamma e^2} \exp(\gamma s(1+\varepsilon)) \tag{6}$$

which is generally linear within the working range of FSS, and can be approximated by

$$R \approx \rho L_0 (1+\varepsilon) = R_0 + \rho L_0 \varepsilon \tag{7}$$

where ρ is the gauge factor of resistance to elongation, R_0 is the initial electrical resistance of FSS, L_0, ε are the initial length of FSS and applied strain, respectively. The above relationship between resistance and strain has been constantly confirmed and utilized by previous works [8, 31, 37].

To connect creep deformation of different sections with variance of electrical resistance, let r_{10}, r_{20}, r_{30} be the initial electrical resistance of spring-dashpots and spring elements, respectively. For fully relaxed FSS without tension, we have

$$r_{10} + r_{20} + r_{30} = R_0 \tag{8}$$

where the summation of sectional resistance equals total initial resistance R_0. Consider a perfect relaxation, i.e., no initial displacement occurs from the strain of ε_0, we have the temporal resistance during relaxation expressed by

$$R(t) = R_0 + \rho_1 s_1 + \rho_2 s_2 + \rho_3 s_3 \tag{9}$$

where ρ_1, ρ_2, ρ_3 are the gauge factor of resistance to elongation of corresponding sections. Hence, once the time-dependent displacements s_1, s_2 are known, the temporal electrical resistance of the FSS can be determined. It can also be easily seen that $\rho L_0 \varepsilon = \rho_1 s_1 + \rho_2 s_2 + \rho_3 s_3$. The above equations and derivations together establish connections from tension to creep deformation of sensing materials, and then the resistance relaxation of FSSs.

Substitute s_1, s_2 with an explicit expression as obtained in the mechanical model of FSS as in (3), the resistance of FSS during relaxation can be obtained in similar form with the same relaxation indices λ_1, λ_2 :

$$R(t) = R(\infty) + r_1 \cdot e^{-\lambda_1 t} + r_2 \cdot e^{-\lambda_2 t} \tag{10}$$

where $R(\infty)$ denotes the limitation of resistance at infinite time, r_i and λ_i are coefficient and relaxation indices, respectively.

2.4 Methods to identify parameters of the electromechanical model

As aforementioned, the time-dependent displacements of pistons of spring-dashpot sections s_1, s_2 serve as the crucial ties between temporal tension F and electrical resistance R of the FSSs. The mechanical and electrical parameters can be identified based on the temporal tension and resistance data provided by the relaxation test (Section 3.1). Through non-linear curve-fitting of the real-time measured tension according to equation (1) based on the least square method, $\sigma(\infty), \sigma_1, \lambda_1, \sigma_2, \lambda_2$ can be directly obtained. To determine the status parameters s_1, s_2, the following 5 simultaneous equations involving the 5 structural parameters, i.e., $k_1, \eta_1, k_2, \eta_2, K$, should be considered.

$$\begin{cases} \lambda_1 = \dfrac{1}{2}\left(\varphi_{11} + \varphi_{12} + \varphi_{21} + \varphi_{22} - \psi\right) \\ \lambda_2 = \dfrac{1}{2}\left(\varphi_{11} + \varphi_{12} + \varphi_{21} + \varphi_{22} + \psi\right) \\ \sigma_1 = \left(k_1 - \eta_1\lambda_1\right) C_{11} \\ \sigma_2 = \left(k_1 - \eta_1\lambda_2\right) C_{12} \\ \sigma(\infty) = \dfrac{l_0}{\dfrac{1}{k_1} + \dfrac{1}{k_2} + \dfrac{1}{K}} \end{cases} \tag{11}$$

Where φ, ψ are the same as in equation (3). Further given another two initial status $s_{1,0}, s_{2,0}$, the above equations can give full determination of the mechanical model of FSS. However, it's not appropriate to solve them from the 5 directly obtained parameters $\sigma(\infty), \sigma_1, \sigma_2, \lambda_1, \lambda_2$, according to equation (11). In this case, other equations involving the tension relaxation at different strains shall be included. Since one data set of tension relaxation would introduce another 2 status parameters s_1, s_2 but at the same time provides another 3 coefficients $\sigma_\infty, \sigma_1, \sigma_2$ (related to the same structural parameters $k_1, \eta_1, k_2, \eta_2, K$) and establish 3 more equations, 3 different strains are theoretically compulsory to give all the mechanical parameters and initial status for the target sensor.

Luckily, since λ_2 was empirically observed as close to zero and η_1 relatively high compared to the stiffnesses, it can be easily derived that status s_1 is always a negligible small value. In this scenario, tensions at 2 different strains are enough to identify all the mechanical parameters and corresponding initial status, based on the following equation set:

$$\begin{cases} \lambda_1 = \dfrac{1}{2}\left(\varphi_{11}+\varphi_{12}+\varphi_{21}+\varphi_{22}-\psi\right) \\ \lambda_2 = \dfrac{1}{2}\left(\varphi_{11}+\varphi_{12}+\varphi_{21}+\varphi_{22}+\psi\right) \\ \sigma_{1,\varepsilon_1} = \left(k_1-\eta_1\lambda_1\right)C_{11,\varepsilon_1} \\ \sigma_{1,\varepsilon_2} = \left(k_1-\eta_1\lambda_2\right)C_{12,\varepsilon_2} \\ \sigma_{2,\varepsilon_1} = \left(k_1-\eta_1\lambda_1\right)C_{11,\varepsilon_1} \\ \sigma_{2,\varepsilon_2} = \left(k_1-\eta_1\lambda_2\right)C_{12,\varepsilon_2} \\ \sigma_{\infty,\varepsilon_1} = \dfrac{l_1}{\dfrac{1}{k_1}+\dfrac{1}{k_2}+\dfrac{1}{K}} \quad \text{or} \quad \sigma_{\infty,\varepsilon_2} = \dfrac{l_2}{\dfrac{1}{k_1}+\dfrac{1}{k_2}+\dfrac{1}{K}} \end{cases} \tag{12}$$

where $\sigma_{i,\varepsilon_n}, C_{ij,\varepsilon_n}$ are the coefficients (under the same definition as in equation (3)) for the tension relaxation released from strain $\varepsilon_n, n=1,2$. The above equation set can properly give all unknown mechanical and status parameters.

To further establish the electrical parameters of the FSS model, the 3 subsections' gauge factors (sensitivity of resistance to strain) shall be further determined. Similarly, the resistance during relaxation can be curve-fitted to identify the parameters of $R(\infty)$, r_1 and r_2 first, according to equation (10). Later, the above coefficients were connected with creep deformation s_1, s_2, while mechanical parameters and the 3 electrical parameters ρ_1, ρ_2, ρ_3 shall be identified, by considering another simultaneous set of equations as below

$$\begin{cases} r_1 = (\rho_1 - \rho_3) C_{11} + (\rho_2 - \rho_3) C_{21} \\ r_2 = (\rho_1 - \rho_3) C_{12} + (\rho_2 - \rho_3) C_{22} \\ R(0) - R_0 = \rho_3 l_0 \quad \text{or} \quad R(\infty) - R_0 = \rho_1 C_{13} + \rho_2 C_{23} + \rho_3 l_0 \end{cases} \tag{13}$$

where the last two equations are equivalent to each other, $R(0)$ is the resistance of stretched FSS before relaxation happened. The parameters on left hands can all be directly obtained from the observed data or through fitting, while right hands of equations are all related to the 3 unknown parameters ρ_1, ρ_2, ρ_3 and other mechanical parameters. The above equation sets are appropriate to determine the all the unknown parameters of the model of FSS.

In the next section, parameters of the mechanical and electromechanical models are to be identified using the temporal tension and electrical resistance measured from the relaxation test at the strain of ε_1. The determined model is then applied to predict the resistance during relaxation at another strain ε_2. Error analysis would then be implemented to evaluate the effectiveness of the determined models, by analyzing the difference between actually measured resistance and predicted resistance. The schematic routine of the model determination and validation is shown in **Figure 3**.

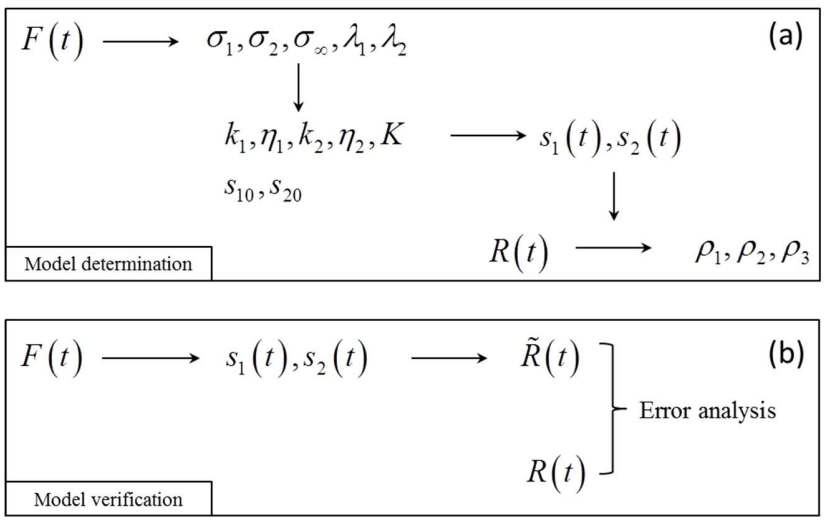

Figure 3. Schematic diagram of the model determination (a) and model application (b)

All fitting and solution process were realized by self-programmed functions and scripts with MATLAB.

3. Experiment and results

3.1 Protocol of the relaxation test and experimental setup

5 FSSs (No.1 ~5) with the sensing area of 8*30 mm^2 belong to 2 batches were randomly selected for this study. In order to derive and verify of the electromechanical model of FSS, relaxation tests were conducted. INSTRON 5944 was used to provide the condition of fixed strain and measure temporal tension of FSSs. Before the relaxation tests, FSS underwent 10 cycles of loading-unloading by INSTRON between 0% strain and 60% strain at a speed of 60mm/min to sufficiently prepare the fibers of samples for stretching and stabilize the strain-resistance property of coating CE of FSSs [8]. After pretreatment, the FSS takes 10 min to rest with no stretching till no more obvious changes in electrical resistance.

To study the stress and resistance relaxation, FSS was fast stretched by INSTRON 5944 to the target strain (e.g., 30%, 60%) and then hold steady for 60 seconds. The ramp speed of INSTRON during stretching was set to as high as 120mm/s. Load (tension) and resistance of FSSs during the test was detected and stored simultaneously by the INSTRON associated with Keithley 2010, with a sampling frequency of 50 Hz.

The experimental setup was similar to that of our previous work [35], only that INSTRON 5944 and Keithley 2010 were utilized as the tensile instrument and data acquisition device.

A demonstration of the original data of tension (for single-axis elongation, tension represents stress.), and resistance variation with respect to time was plotted in **Figure 4**. The data belongs to sample No.1 during the relaxation test of 30% strain.

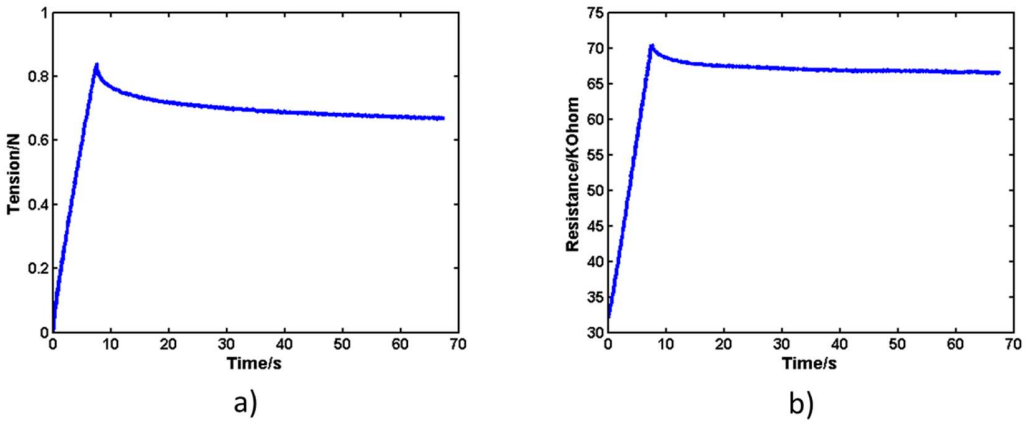

Figure 4. Raw data of tension a) and resistance b) obtained during the relaxation test

It can be clearly seen from the figure that the while FSS maintained a constant strain during hold, both tension and resistance decreased simultaneously with time. Meanwhile, the speed/rate of decreasing in tension and resistance also reduced with time.

3.2 Identification of mechanical and electrical parameters

Physical significance and mechanism of the newly proposed model have been elaborated above. The three coefficients $\sigma(\infty), \sigma_1, \sigma_2$, and two relaxation indices λ_1, λ_2 can be directly fitted with the temporal tension. According to equation (3), the relaxation indices λ_1, λ_2 take no effect from the unknown status s_1, s_2 as well as the initial elongation l_0 and thus can be utilized as a preliminary indicator of the validity of the model. Each FSS was tested in relaxation at two different strain levels, 30% and 60%, the fitted parameters can be retrieved and summarized in **Table 1**.

Table 1 Directly identified parameters using temporal tension relaxation at different strain levels

Sample	Strain level	$\sigma(\infty)$	σ_1	σ_2	λ_1	λ_2
FSS	30%	0.8044	0.0759	0.0955	0.8219	0.04563
No.1	60%	1.5909	0.1458	0.1818	0.8049	0.04740
FSS	30%	0.8324	0.0907	0.1134	0.7878	0.04658
No.2	60%	1.6652	0.1729	0.2229	0.7854	0.04536
FSS	30%	0.7177	0.0489	0.0781	0.7781	0.04767
No.3	60%	1.5710	0.1473	0.1829	0.8158	0.04904
FSS	30%	0.6659	0.0743	0.0989	0.8124	0.04869
No.4	60%	1.3440	0.1324	0.1692	0.8368	0.04668
FSS	40%	0.9393	0.1003	0.1248	0.9989	0.04670
No.5	60%	1.4204	0.1473	0.1729	0.9850	0.04700

The model fits well for relaxation data, with all goddesses of fittings (r^2) exceed the high value of 0.9960, as demonstrated in **Figure 5**, confirming that 2 relaxation indices are good enough to characterize the decreasing of tension in short future (within 60s). Furthermore, it can be seen that the relaxation indices λ_1 and λ_2 generally maintained certain values, with a max discrepancy of 3% for λ_1 and 4.3% for λ_2, preliminary accords with the proposed model. Generally, those obtained in the larger strain of 60% were kept for later identification of structural parameters of the model. This is to avoid large fitting errors while extracting the above parameters since both the signals of temporal measured tension and trends of curves were more obvious at the larger strain. Meanwhile, the value of λ_1 is 20 times the value of λ_2, which is about close to zero, indicating a relatively high damping coefficient of η_1 according to equation (13).

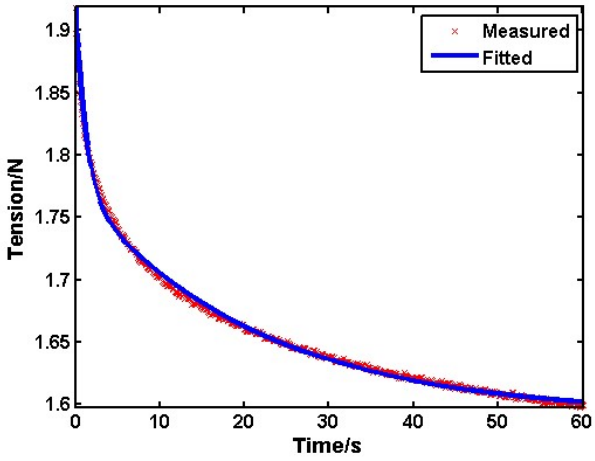

Figure 5. For demonstration of parameter extraction: curve fitting of tension relaxation of FSS No.1 at 60% strain.

As aforementioned, data of tension relaxation at 30% and 60% strains were to be included to identify all the electromechanical parameters and corresponding initial status. To facilitate the solution of equations and searching of the roots, a 3-step scheme was considered. Firstly, the 5 mechanical parameters were preliminarily estimated according to equation (4), under the assumption that initial status $s_{1,0}, s_{2,0}$ are forced to be zero. Then, the 5 mechanical parameters and 4 initial status at 2 strain levels were solved according to equation (12), searched from the initial start point of the estimated parameters from step 1. Last, with temporal electrical resistance at 30% strain, another searching was started from the mechanical and status parameters obtained from step 2, for determining all parameters according to equation set (13).

The parameters as well as initial status obtained from the 2nd and 3rd steps were summarized in **Table 2** and **Table 3**, respectively.

Table 2. Identified mechanical parameters of the FSS (step 2)

	k_1 N/mm	η_1 N.s/mm	k_2	η_2	K	$s_{1,0}$	s_{1,ε_1}	$s_{2,0}$	s_{2,ε_2}
FSS No.1	1.1198	26.8702	1.3126	1.7751	0.1290		0.0933		0.2401
FSS No.2	1.0606	26.1734	0.9633	1.4035	0.1423		0.3512		0.7628
FSS No.3	1.1486	26.5290	1.1432	1.6051	0.1256	0	0.3746	0	0.3543
FSS No.4	1.0107	24.0153	0.3865	0.6294	0.1315		1.1464		2.9539
FSS No.5	1.0738	25.6492	0.7252	0.8640	0.1314		0.4172		1.2367

Table 3. Identified mechanical and electrical parameters of the FSS (step 3)

	k_1 N/mm	η_1 N.s/mm	k_2	η_2	K	$s_{1,0}$	s_{1,ε_1}	$s_{2,0}$	s_{2,ε_2}	ρ_1	ρ_2	ρ_3
FSS No.1	1.1193	26.8586	1.3413	1.8102	0.1287		0.0377		0.2401	3.8803	1.8155	6.0014
FSS No.2	1.0611	26.1852	0.9593	1.3986	0.1424		0.3939		0.7492	4.1415	2.1816	6.4305
FSS No.3	1.1574	26.7331	1.1796	1.6619	0.1249	0	0.1745	0	0.3867	5.3339	1.4075	8.4353
FSS No.4	0.9898	23.5217	0.8051	1.1145	0.1120		0.2502		0.7783	2.1751	2.2865	5.2135
FSS No.5	1.0708	25.5989	1.0603	1.1951	0.1245		0.0091		0.6818	1.2403	1.3720	4.1386

The mechanical parameters shall be consistent in value. However, there is apparent difference in mechanical parameters (especially for k_2, η_2, s_2) for FSS No.4 and 5 between 2nd and 3rd steps, larger than other sensors. The reason can be attributed to that the last 2 sensors belonged to a different sample batch from the first 3.

It can be seen from Table 3 **t**hat for the tested FSSs, the structural parameters are close to each other, while the gauge factor of electrical resistance to strain was observed with higher variance, ranging from 4.1 Khom to 8.4 Khom. FSS No.4 and No.5 were observed with a higher relative reduction of resistance during relaxation ($\Delta R / R_0$), which is in accordance with the relatively higher initial statuses caused by the lower stiffness and damping coefficients of the 2nd spring-dashpot element.

3.3 Verification of the electromechanical model of FSSs

Once the mechanical, electrical parameters as well as status parameters are identified, the model of FSS is established, which can be used to predict responses of FSS subsequently. In this work, the tension relaxation at 30% and 60% strain were used to identify the model's structural parameters and initial statuses. The resistance relaxation at strain of 30% was used to determine the gauge factor ρ_1, ρ_2, ρ_3 of the 3 subsections. The established model will be implemented to calculate the variation of resistance during relaxation at 30% strain, which would be compared with the real measured temporal resistance. The difference between predicted and measured resistance would be analyzed for verification of the model.

With the measured resistance and predicted resistance were plotted and compared in **Figure 6**, demonstrated by FSS No.1. The errors were indicated by the maximum error, mean, and standard deviation of error, the mean square error. The correlation and determination coefficient between the predicted resistance and measured resistance was compared to that between measured tension and resistance since many previous works arbitrarily considered tension and resistance vary in a similar way during relaxation. For the 5 FSSs, the error indicators were computed and summarized in **Table 4**. The predicted and measured resistances at 60% strain were compared in **Figure 6**, along with the comparison of the normalized measured tension and resistance.

Table 4. Error indicators between measured and predicted resistance during relaxation at 60 % strain

	Max.error (Khom)	Mean.error (Khom)	Std (Khom)	Mse (Khom)	Cor. Coef *1	Cor.Coef *2	R^2 *3	R^2 *4
FSS No.1	0.6476	0.1018	0.2206	0.0590	0.9392	0.9749	0.5954	0.9379
FSS No.2	0.8038	0.1430	0.2287	0.0727	0.9298	0.9774	0.6521	0.9363
FSS No.3	1.2756	0.3101	0.4045	0.2595	0.8870	0.9602	0.4166	0.8694
FSS No.4	0.5382	0.0991	0.1716	0.0392	0.9368	0.9887	0.8013	0.9689
FSS No.5	0.6260	0.2894	0.1643	0.1107	0.9833	0.9904	0.5507	0.9025

*1 The correlation between measured tension and resistance; *2 The correlation between the predicted and measured resistance; *3 Determination coefficient (R^2) of using

measured tension to characterize the resistance relaxation; *4 Determination coefficient (R^2) of using the model to characterize the resistance relaxation.

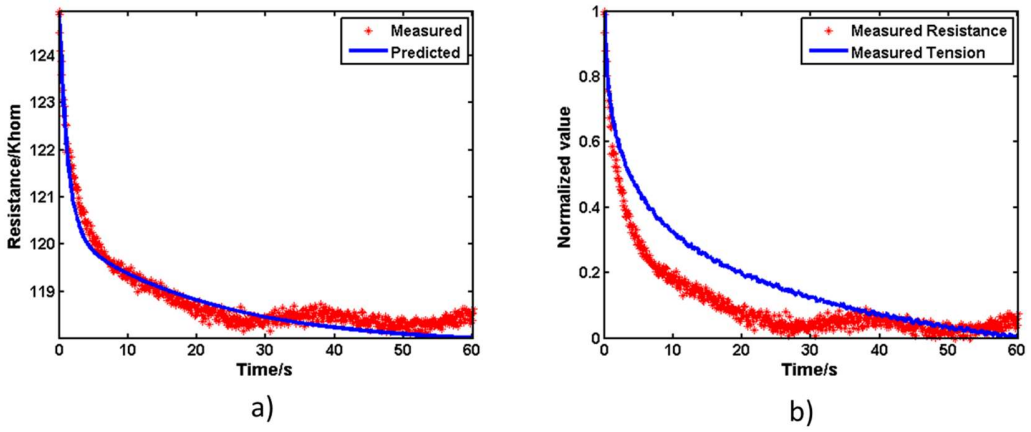

Figure 6. Typical demonstration of model verification: the comparison between measured and predicted resistance a) as well as that between normalized tension and resistance b). The data belongs to FSS No.1 at the 60 % strain.

It can be seen from the table that the max error of 1.2756 Khom between measured and predicted resistance occurred for FSS No.3. This is because FSS No.3 has high initial resistance (48 Khom, and released from 173 Khom), a higher gauge factor (averaged 7.99 Khom/mm), both could lead to a higher variation of resistances. The mean error is 0.1887 Khom (relatively 0.2%), with the averaged determination of fit of 0.9230. These results indicate that the model is effective to characterize the variation of both the stress and resistance during relaxation. To show the model is much more effective to predict or characterize the resistance relaxation than just according to the similarity between curves of stress and resistance relaxation [14, 19, 34], correlations between predicted and measured resistance have been calculated and found with an averaged value of 0.9783, significantly higher than that between measured tension and resistance (averaged 0.9352). The averaged determination coefficient 0.9230 is also much higher than that when using stress relaxation to characterize the resistance relaxation (averaged 0.6032).

4. Discussions

As shown in above, the proposed electromechanical model has established a clear connection between stress relaxation and resistance relaxation for sensors based on conductive polymers. Once the mechanical, electrical as well as status parameters of the model are determined, resistance error caused by creep of conductive polymers can theoretically be evaluated and compensated. Furthermore, with sensor fusion technology such as the Kalman filtering method, it's feasible to solve the real temporal stimulation, i.e., the applied strain, through estimating the status parameters from an array of coupled sensors. This would be a potential solution for polymer sensors to give accurate measurements, especially for urgent demanded wearable applications such as accurate tracking of human joint angles or motion styles for diagnoses or rehabilitations purposes.

However, it should be pointed out that the aside from the status parameters, which are influenced by loading history, the mechanical or electrical parameters may also vary. As an energy input-output system, the steady-state intrinsic energy or temperature of the sensor is jointly-governed by styles of extension (speed, strain, etc., related to intensity of intermolecular friction) and speed of heat dissipation. Hence, pretreatment and determining the current parameters for the model are both suggested as compulsory. Otherwise, the real-estate electromechanical property, such as gauge factor of resistance to strain, may shift with time, indicating instability of electromechanical parameters. To illustrate this, FSS No.6 further started from no pretreatment and underwent consecutive relaxation tests as indicated in **Figure 7a**.

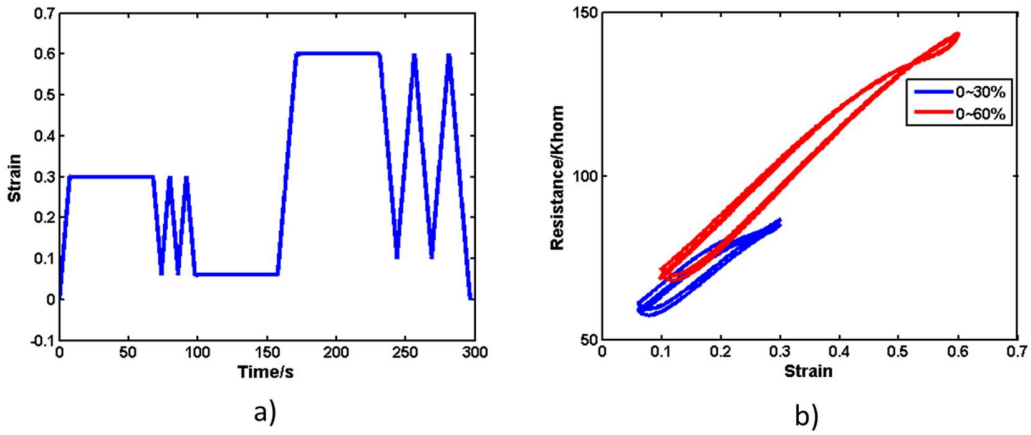

Figure 7. (a)Test protocol of FSS No.6 and (b) Difference of strain-resistance properties between the working range of 0~30% and 0~60%

Unlike the previous test, 2.5 cycles of elongations for determination of gauge factor followed each relaxation tests. It was found that the 2 tension relaxations along with resistance relaxations cannot give a solution of electromechanical and status parameters. It was then observed that the overall gauge factor of resistance to strain significantly changed, from 2.8718 Khom/mm to 3.2421 Khom/mm, with a relative rising of as high as 13%, as shown in **Figure 7b**. This basically failed the assumption of modeling since the electromechanical properties have shifted. Hence, to make the model applicable, stabilization by pretreatment as well as determination of current electromechanical parameters are necessary.

5. Conclusion

In this paper, mechanical and electrical relaxations of CE fabric strain sensors based on carbon-particle-filled polymer and knitted fabric substrate were studied through electrical and mechanical modeling. A serial mechanical model of CE fabric strain sensors was firstly proposed. Sectional gauge factors and status parameters were then included to provide an electromechanical mechanism of the FSSs. The model was determined for each FSS through parameter identification and applied for prediction of variance in resistance for FSS during relaxation.

Results show that the relative mean error of the predicted resistance by the model was only 0.2%, with the averaged determination of fit 0.9230, much higher than that when using stress relaxation to characterize the resistance relaxation (averaged 0.6032). Moreover, the correlation and determination coefficient between predicted and measured resistance was observed 0.9783 on average, higher than that between measured tension and resistance (0.9352). Hence, the model is effective to reveal the sensing mechanism and characterize the resistance relaxation of the sensors, other than using the stress relaxation as in previous works. These findings reveal that creep deformation of different subsections was the reason of the resistance relaxation. In this perspective, higher elasticity and lower damping coefficient of the sensing area shall diminish the resistance relaxation. Unlike previously published works, this simple but effective model is derived based on parameters with physical significance, other than phenomenological similarity.

It's suggested that the validity of using the model to predict later electromechanical behavior of FSSs highly depends on the stability of the electromechanical property, such as the gauge factor of resistance to strain.

Generally, the methods and results of this work will inspire characterizing the resistance relaxation of other flexible sensors based on conductive polymers. To enhance the potential of the model in providing accurate measurements of strains, further study of the model's responses under dynamic stretching has been scheduled in future work.

Acknowledgment

Funding: This research was funded by the National Natural Science Foundation of China (Grant No. 12002085, 51603039), sponsored by the Shanghai Pujiang Program, supported by the Fundamental Research Funds for the Central Universities, the Key Laboratory of Textile Science and Technology (Donghua University), Ministry of Education, and the Initial Research Funds for Young Teachers of Donghua University.

Conflicts of Interest: The authors declare no conflict of interest.

References

1. Zhan, C.X., et al., *Conductive polymer nanocomposites: a critical review of modern advanced devices.* Journal of Materials Chemistry C, 2017. **5**(7): p. 1569-1585.
2. Ryu, S., et al., *Extremely Elastic Wearable Carbon Nanotube Fiber Strain Sensor for Monitoring of Human Motion.* Acs Nano, 2015. **9**(6): p. 5929-5936.
3. Yip, M.C. and G. Niemeyer, *On the Control and Properties of Supercoiled Polymer Artificial Muscles.* Ieee Transactions on Robotics, 2017. **33**(3): p. 689-699.
4. Zhan, Z.Y., et al., *Paper/Carbon Nanotube-Based Wearable Pressure Sensor for Physiological Signal Acquisition and Soft Robotic Skin.* Acs Applied Materials & Interfaces, 2017. **9**(43): p. 37921-37928.
5. Zhou, Z.Q., et al., *Supersensitive all-fabric pressure sensors using printed textile electrode arrays for human motion monitoring and human-machine interaction.* Journal of Materials Chemistry C, 2018. **6**(48): p. 13120-13127.
6. McLaren, R., et al., *A review of e-textiles in neurological rehabilitation: How close are we?* Journal of Neuroengineering and Rehabilitation, 2016. **13**: 59.
7. Liu, H., et al., *Electrically conductive polymer composites for smart flexible strain sensors: a critical review.* Journal of Materials Chemistry C, 2018. **6**(45): p. 12121-12141.
8. Wang, X., et al., *Monitoring elbow isometric contraction by novel wearable fabric sensing device.* Smart Materials and Structures, 2016. **25**(12).
9. Wang, X., X.M. Tao, and R.C.H. So, *A Bio-mechanical Model for Elbow Isokinetic and Isotonic Flexions.* Scientific Reports, 2017. **7**: 8919.
10. Tognetti, A., et al., *Wearable Goniometer and Accelerometer Sensory Fusion for Knee Joint Angle Measurement in Daily Life.* Sensors, 2015. **15**(11): p. 28435-28455.
11. Meng, F.L., R.H. Pritchard, and E.M. Terentjev, *Stress Relaxation, Dynamics, and Plasticity of Transient Polymer Networks.* Macromolecules, 2016. **49**(7): p. 2843-2852.
12. Reynolds, C., R. Thompson, and T. McLeish, *Pressure and shear rate dependence of the viscosity and stress relaxation of polymer melts.* Journal of Rheology, 2018. **62**(2): p. 631-642.
13. Askar, S., C.M. Evans, and J.M. Torkelson, *Residual stress relaxation and stiffness in spin-coated polymer films: Characterization by ellipsometry and fluorescence.* Polymer, 2015. **76**: p. 113-122.
14. Zhai, T.L., et al., *Piezoresistive and compression resistance relaxation behavior of water blown carbon nanotube/polyurethane composite foam.* Composites Part a-Applied Science and Manufacturing, 2015. **72**: p. 108-114.
15. Can-Ortiz, A., J.L. Abot, and F. Aviles, *Electrical characterization of carbon-based fibers and their application for sensing relaxation-induced piezoresistivity in polymer composites.* Carbon, 2019. **145**: p. 119-130.
16. Voet, A., F. Cook, and A. Sircar, *Relaxation of stress and electrical resistivity in carbon-filled vulcanizates at minute shear strains.* Rubber Chemistry and Technology, 1971. **44**(1): p. 175-184.
17. Voet, A., *Temperature effect of electrical resistivity of carbon black filled polymers.* Rubber Chemistry and Technology, 1981. **54**(1): p. 42-50.
18. Kost, J., A. Foux, and M. Narkis, *Quantitative Model Relating Electrical-Resistance, Strain, and Time for Carbon-Black Loaded Silicone-Rubber.* Polymer Engineering and Science, 1994. **34**(21): p. 1628-1634.
19. Ding, T.H., L.H. Wang, and P. Wang, *Changes in electrical resistance of carbon-black-filled silicone rubber composite during compression.* Journal of Polymer Science Part B-Polymer Physics, 2007. **45**(19): p. 2700-2706.

20. Wang, L.H., T.H. Ding, and P. Wang, *Effects of instantaneous compression pressure on electrical resistance of carbon black filled silicone rubber composite during compressive stress relaxation.* Composites Science and Technology, 2008. **68**(15-16): p. 3448-3450.
21. Wang, L.H., T.H. Ding, and P. Wang, *Research on stress and electrical resistance of skin-sensing silicone rubber/carbon black nanocomposite during decompressive stress relaxation.* Smart Materials and Structures, 2009. **18**(6).
22. Wang, L.H., et al., *Study on compressive resistance creep and recovery of flexible pressure sensitive material based on carbon black filled silicone rubber composite.* Sensors and Actuators a-Physical, 2011. **165**(2): p. 207-215.
23. Wang, L.H. and Y.Y. Han, *Compressive relaxation of the stress and resistance for carbon nanotube filled silicone rubber composite.* Composites Part a-Applied Science and Manufacturing, 2013. **47**: p. 63-71.
24. Zhang, X.W., et al., *Time dependence of piezoresistance for the conductor-filled polymer composites.* Journal of Polymer Science Part B-Polymer Physics, 2000. **38**(21): p. 2739-2749.
25. Zheng, Q., J.F. Zhou, and Y.H. Song, *Time-dependent uniaxial piezoresistive behavior of high-density polyethylene/short carbon fiber conductive composites.* Journal of Materials Research, 2004. **19**(9): p. 2625-2634.
26. Cao, Q., et al., *Conductive and viscoelastic behaviors of carbon black filled polystyrene during annealing.* Carbon, 2010. **48**(15): p. 4268-4275.
27. Shangguan, Y.G., et al., *New Insight into Time-Temperature Correlation for Polymer Relaxations Ranging from Secondary Relaxation to Terminal Flow: Application of a Universal and Developed WLF Equation.* Polymers, 2017. **9**(11): 567.
28. Zhang, Y.X., et al., *Dynamic rheology and dielectric relaxation of poly(vinylidene fluoride)/poly(methyl methacrylate) blends.* Composites Science and Technology, 2015. **106**: p. 39-46.
29. Chen, Q., et al., *Mechanical Reinforcement of Polymer Nanocomposites from Percolation of a Nanoparticle Network.* Acs Macro Letters, 2015. **4**(4): p. 398-402.
30. Wang, F., et al., *Flexible pressure sensors for smart protective clothing against impact loading.* Smart Materials and Structures, 2014. **23**(1).
31. Shu, L., et al., *In-Shoe Plantar Pressure Measurement and Analysis System Based on Fabric Pressure Sensing Array.* Ieee Transactions on Information Technology in Biomedicine, 2010. **14**(3): p. 767-775.
32. Yamaguchi, K., J.J.C. Busfield, and A.G. Thomas, *Electrical and mechanical behavior of filled elastomers. I. The effect of strain.* Journal of Polymer Science Part B-Polymer Physics, 2003. **41**(17): p. 2079-2089.
33. Wang, L.H., T.H. Ding, and P. Wang, *Influence of carbon black concentration on piezoresistivity for carbon-black-filled silicone rubber composite.* Carbon, 2009. **47**(14): p. 3151-3157.
34. Wang, L.H., C.G. Xu, and Y.L. Li, *Piezoresistive response to changes in contributive tunneling film network of carbon nanotube/silicone rubber composite under multi-load/unload.* Sensors and Actuators a-Physical, 2013. **189**: p. 45-54.
35. Gao, Y., et al., *Characterizing the Resistance Relaxation of the Fabric-based Resistive Sensors Based on an Electro-mechanical Model.* Sensors and Actuators A: Physical, 2020. **310**: p. 112041.
36. Simmons, J.G., *Electric tunnel effect between dissimilar electrodes separated by a thin insulating film.* Journal of applied physics, 1963. **34**(9): p. 2581-2590.
37. Wang, Y.Y., et al., *Novel fabric pressure sensors: design, fabrication, and characterization.* Smart Materials & Structures, 2011. **20**(6).